Characterization of Finite-Width Ground Coplanar Waveguides on High Resistivity Silicon With Ultralow Metallization Thickness

Jarosław Judek, Arkadiusz P. Gertych, Michał Świniarski, Mariusz Zdrojek, Jerzy Krupka, and Jerzy K. Piotrowski

***Abstract*— In this paper, we report the microwave properties of finite-ground coplanar waveguides (CPWs) fabricated on a thermally oxidized high resistivity silicon substrate. The ultralow metallization thickness indicates a gold metallization with a thickness in the range from 10 to 100 nm. We present measured magnitudes and phases of the S_{11} and S_{21} parameters of the CPW segments in the frequency range from 0.1 to 26 GHz, which are transformed based on the signal flow graph to the characteristic impedance Z_0, the attenuation coefficient α, and the effective dielectric constant ε_{eff}. We analyze the CPW attenuation dependence on the metallization thickness based on the $\alpha(f) = \alpha_0 \cdot (f/1\ \text{GHz})^n$ model.**

***Index Terms*— Attenuation, conductor losses, coplanar waveguide (CPW), high-frequency measurements, high resistivity silicon (HRS) substrate.**

I. Introduction

COPLANAR waveguide (CPW) is a well-known planar transmission line of the microwave technique. Due to its many advantages, CPW is commonly used to convey electric signals in the gigahertz frequency range. Currently, CPW is used as a part of monolithic microwave integrated circuits, parallel and series microwave passive components and often comprises the input–output circuitries of various RF devices, such as high-speed transistors or ultrafast photodetectors. The robustness of CPW originates in the well-understood principle of operation and effective simulation algorithms that allow for reliable design. However, in a typical CPW, the metallization thickness is on the order of micrometers, which is hardly achievable using many modern nanofabrication techniques, such as those based on electron beam lithography and lift-off processes, where the height of the metallic structures rarely exceeds 100 nm [1], [2]. In the situation where the metallization thickness is on the nanometer scale, the following three problems immediately arise: 1) the microwave losses proportional to the sheet resistance of the metallization R_S greatly increase due to the $R_S = 1/\sigma \cdot t$ dependence; 2) the conductivity of the metallic layer σ decreases with the decreasing thickness value t; and 3) the metallization thickness t is lower than the skin depth δ value, which, for bulk gold at $f = 10$ GHz, is approximately 0.79 μm. The third issue is especially interesting because it implies the question of whether the ultrathin metallic layer still acts as a metal that imposes particular electromagnetic field boundary conditions or it is more proper to describe it as a semi-transparent lossy dielectric medium.

In this paper, we characterize CPWs fabricated on a thermally oxidized high resistivity silicon (HRS) wafer using Cr/Au metallization, where the thickness of the Cr adhesive layer t_{Cr} is 5 nm, and the thicknesses of the Au layer t_{Au} are 10, 20, 30, 50, 70, and 100 nm. We provide measurement results of the S-matrix components in the frequency range from 0.1 to 26 GHz. The transformation of the measured S-parameters into the characteristic impedance Z_0 and the propagation constant γ of the CPW under testing is based on the signal flow graph between the probe tips of the probe station.

The properties of the coplanar waveguides (CPWs) on HRS substrates, including the CPW attenuation problem with respect to the substrate resistivity, the dielectric layer and surface carrier problems on the SiO_2/Si interface, or the methods of improving CPW performance, have widely been reported in the literature [3]–[14]. The problems of lossy metallization, metallization with finite thickness or finite-extent grounds have also been examined [15]–[19]. However, according to the authors' knowledge, the frequency characteristics of the CPW parameters on silicon with an ultralow gold metallization thickness (10 nm $\leq t_{\text{Au}} \leq$ 100 nm) are presented for the first time. The most similar reports concern the attenuation of CPW made from 250-nm-thin gold film on InP [16], [17] and losses of CPW made from 200-nm-thin aluminum film on glass [19].

II. CPW Fabrication

The structure of the finite-width ground metallization CPW used in this paper is shown in Fig. 1. The width of the central strip $W_1 = 100$ μm and the gap $G = 50$ μm were chosen to both fit the dimensions of a microwave

Manuscript received October 19, 2016; revised April 14, 2017; accepted July 1, 2017. Date of publication August 8, 2017; date of current version December 12, 2017. This work was supported by the National Centre for Research and Development within the projects under Grant Graftech/NCBR/13/20/2013 and Grant Lider/180/L-6/14/NCBR/2015. *(Corresponding author: Jarosław Judek.)*

J. Judek, A. P. Gertych, M. Świniarski, and M. Zdrojek are with the Faculty of Physics, Warsaw University of Technology, 00-662 Warsaw, Poland (e-mail: jerryj@if.pw.edu.pl).

J. Krupka and J. K. Piotrowski are with the Institute of Microelectronics and Optoelectronics, Faculty of Electronics and Information Technology, Warsaw University of Technology, 00-662 Warsaw, Poland (e-mail: piotrowski@imio.pw.edu.pl).

Color versions of one or more of the figures in this paper are available online at http://ieeexplore.ieee.org.

Digital Object Identifier 10.1109/TMTT.2017.2731954

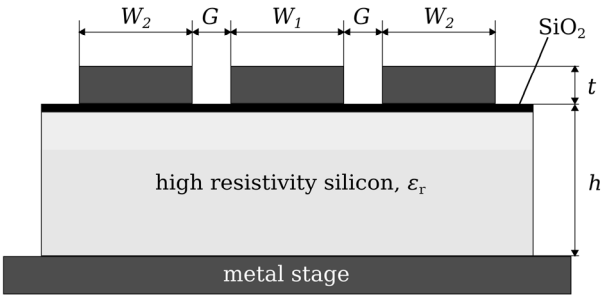

Fig. 1. Schematics of finite-ground CPWs used in this paper. $W_1 = 100\ \mu$m, $G = 50\ \mu$m, $W_2 = 100$ or $300\ \mu$m, $h = 525\ \mu$m, and $t = t_{Cr} + t_{Au}$, thickness of the SiO_2 dielectric layer is 50 nm.

probe with 150-μm pitch and to obtain the characteristic impedance of approximately 50 Ω at 10 GHz for the 5-nm Cr + 100-nm Au metallization. The width of the ground planes is set to one or three times the width of the central strip, i.e., 100 or 300 μm. The CPW is placed on the metal stage of the probe station; however, there is no backside metallization.

HRS wafers [20]–[25] (flat zone method, diameter 4 in, thickness 525 μm, orientation 100, boron doping, one side polished, $\rho \geq 20$ kΩ·cm, and $\varepsilon_r = 11.65$ [26]) were used as the substrate. Prior to the metal deposition, all wafers were thermally oxidized to produce a 50-nm-thick SiO_2 dielectric layer. The microwave resistivity of the oxidized wafers, found using a microwave split-post dielectric resonator operating at approximately 4.5 GHz [27], equals approximately 1 kΩ · cm, which is more than 20 times less than the resistivity of pristine wafers. It was reported that the SiO_2 dielectric layer on the surface of the HRS wafers increases the microwave dissipation losses and deteriorates the CPW properties [9], [10], [20], [21]. However, the dielectric layer prevents unintentional dc leakage current.

The metallic structures were fabricated using electron beam lithography and a lift-off process. The Cr and Au layers were deposited by resistive thermal evaporation under the pressure of 1×10^{-6} Torr. All structures were inspected using an atomic force microscope to confirm their thickness and quality. The measured thicknesses are equal to the designed ones within the 1-nm-uncertainty limit. The root mean square (RMS) of the height of the metallization—a measure of roughness, calculated for 10 μm × 10 μm square map of 10-nm resolution, is below 0.8 nm for all samples, in accordance with [19]. However, this is only an estimate of the upper limit of the true RMS value due to instrumental limitations. The sheet resistance R_S of each metallization thickness was determined twice: for the direct current and at the microwave frequency. The results are presented in Table I. The dc measurements were performed using the Transfer Length Method by fabrication of a series of five metal strips of different lengths with constant widths. Exemplary results and a typical structure for 5-nm Cr + 100-nm Au metallization are shown in Fig. 2. Derivative of the resistance of a structure with respect to its aspect ratio (length divided by width) gives the sheet resistance. High aspect ratio values ($L/W = 1000, 1800, 2600, 3400, 4200$) were chosen to minimize the strength of the electric current flowing through the ultrathin metallic structure. The RF measurements were performed using a microwave single-post dielectric resonator

TABLE I
METALLIZATION SHEET RESISTANCE

#	metallization	$R_{S,DC}$ [Ω/□]	$R_{S,RF}$ [Ω/□]
1	5 nm Cr + 10 nm Au	6.86	8.69
2	5 nm Cr + 20 nm Au	2.53	2.91
3	5 nm Cr + 30 nm Au	1.44	1.73
4	5 nm Cr + 50 nm Au	0.710	0.814
5	5 nm Cr + 70 nm Au	0.487	0.528
6	5 nm Cr + 100 nm Au	0.326	0.346

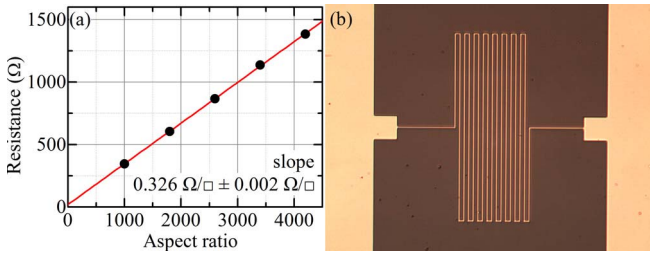

Fig. 2. (a) Resistance of the thin metallic strip versus the aspect ratio (length divided by width); slope equals the sheet resistance. (b) Picture of one of the metallic structures used in the Transfer Length Method for determining the metallization dc sheet resistance for 5-nm Cr + 100-nm Au metallization.

operating at approximately 4.5 GHz [27]. The active area of the microwave resonator is of the order of few cm^2; therefore, for this measurement, whole oxidized HRS wafers were covered entirely by the continuous metallic layers. The obtained sheet resistance values are in a good agreement with the dc counterparts and indicate a slight increase with the frequency (10%–20%).

Increase in the metalization resistivity with decrease in the thickness, as shown in Table I, results from the $1/\sigma \cdot t$ dependence and from simultaneous decrease in the σ value, because at the nanometer scale $\sigma = \sigma\ (t)$. Whereas the former one is a simple function of thickness, the latter one strongly depends on the technological details. Fortunately, in our case, it was possible to grasp which structural or morphological parameter of thin metallic film is responsible for the decrease in σ value. SEM images composing Fig. 3 qualitatively but clearly illustrate increase in size of single grains along with increase in the metallization thickness. Our finding is consistent with other literature reports. For example, Barnat *et al.* [28] observed that the dc electrical resistivity of copper films strongly depends on the film's thickness for thicknesses below the bulk mean free path of copper ~39 nm. Furthermore, he concluded that the average grain size, as opposed to interface roughness, plays a dominant role in the electrical resistivity. In another work, Salvadori *et al.* [29] shown that the average grain size in Au thin films increases along with the metallization thickness, and the saturation of the grain size occurs for film thickness of 140 nm, with a maximum grain size of approximately 48 nm. The last fact particularly emphasizes significance of our study because changes in properties of CPW fabricated using an ultralow Au metallization (10 nm $\leq t_{Au} \leq$ 100 nm) will partially be related to the changes in metallization microstructure.

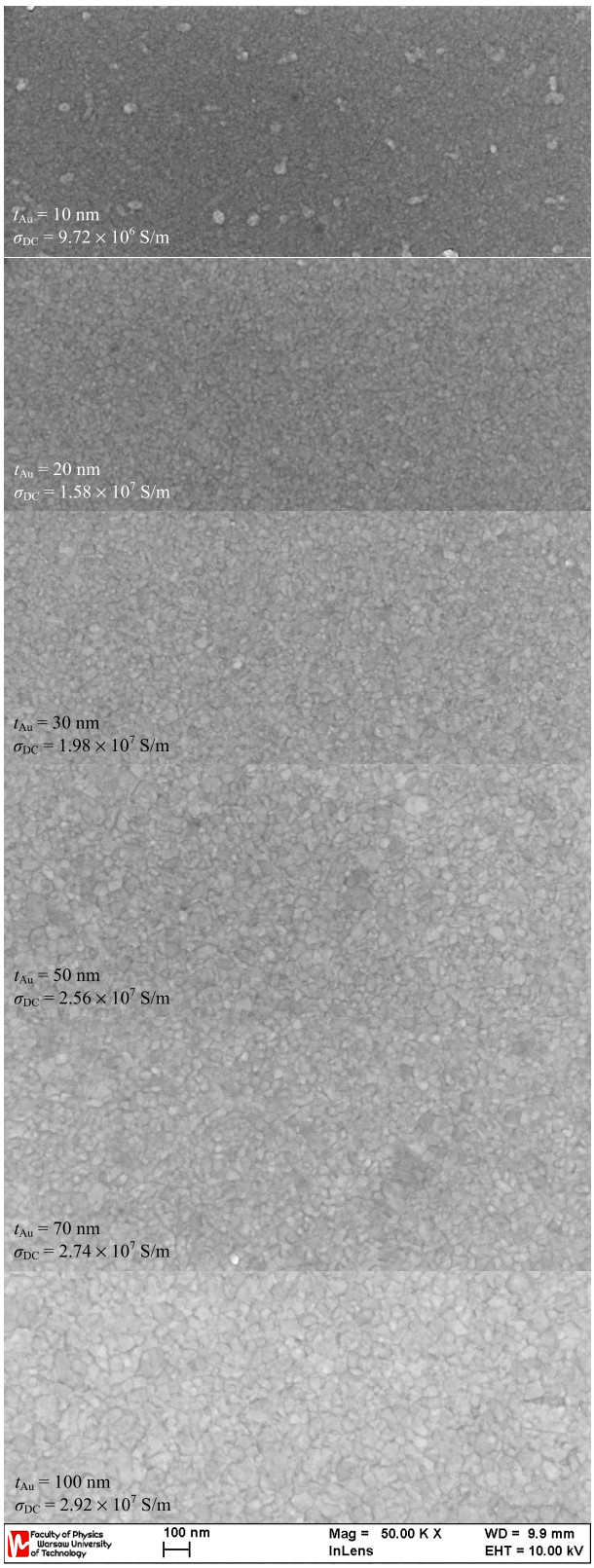

Fig. 3. SEM images illustrating evolution of the microstructure of the metallization along with the metallization thickness.

III. S-Matrix Measurements and CPW Parameter Extraction

The measurement system consisted of a Cascade Microtech PM5 probe station, $|Z|$ Probe 40-K3N-GSG-150 probes, a CRC-8 GSG 100-250 calibration substrate, WinCal XE calibration and measurement software [30], and high-performance phase stable cables. The vector network analyzer was an Agilent N5242A PNA-X.

The enhanced Line–Reflect–Reflect–Match [31], [32] calibration technique of a vector network analyzer was used for placement of the measurement reference planes T_1 and T_2 ahead of the probes contact tips for Ports 1 and 2, respectively. According to [31], [32] a nominal reference characteristic impedance Z_R of 50 Ω is seen at the reference planes.

The S-matrix measurements of the 4 mm long CPW segment, i.e., a two-port network placed between Ports 1 and 2, were performed for all six gold metallization thicknesses and two finite-ground widths. Each measured structure between the probes contact tips is symmetrical; therefore, the reflectance S_{11} at the T_1 plane should be equal to the reflectance S_{22} at the reference plane T_2. The comparison of the measured reflectances indicates that they do not vary appreciably, not more than 40% above the magnitude and phase uncertainties of the network analyzer given in [33]. The measured two-port networks are reciprocal; thus, the forward path transmittance S_{21} (from T_1 to T_2) is equal to the reverse path transmittance S_{12} with the accuracy of the measurement uncertainties of the analyzer. All results of the S_{11} and S_{21} measurements are presented in Fig. 4.

The measured transmittances and magnitudes of reflectances of CPWs with a finite-ground width equal to 100 μm differ only slightly, as compared to CPWs with $W_2 = 300$ μm. As shown in Fig. 4, the significant differences between reflectance phases of CPWs with $W_2 = 100$ and 300 μm are observed for frequencies above 10 GHz and the gold metallization thicknesses of 50, 70, and 100 nm. In these cases, the magnitude of S_{11} is less than 0.08, and the phase uncertainty exceeds 10° and increases rapidly with a decrease in magnitude. The $|S_{11}|$ and $|S_{21}|$ characteristics of CPWs with $W_2 = 300$ μm are smoother than for $W_2 = 100$ μm.

The characteristics in Fig. 4 show the strong influence of the metallization thickness on S_{11} and S_{21}. The best performance is for the CPW with $t = 100$ nm, when more than 50% of the power is transmitted by the 4 mm long CPW and less than 4% is reflected. The worst case is for the CPW with $t = 10$ nm, when only 4% at 1 GHz and 0.25% at 20 GHz of the power is transmitted through the transmission line and 60% at 1 GHz and 10% at 20 GHz of the power is reflected. Thus, the presented results indicate that all investigated transmission lines are lossy or very lossy. Additionally, the S-parameter dispersion shown in Fig. 4 decreases with increasing metallization thickness.

The problem of extracting the planar transmission line parameters from measured S-parameters of on-wafer test structures has widely been reported in the literature [34]–[40]. The main differences in the probe-tip-to-line geometry and substrate permittivity between the measurement and calibration wafers require special measurement techniques and calculation procedures to accurately characterize transmission line parameters.

The measured CPWs shown in Fig. 1 are fabricated on silicon, and the substrate of the CRC-8 calibration structure is Al_2O_3. Thus, there is no significant difference between

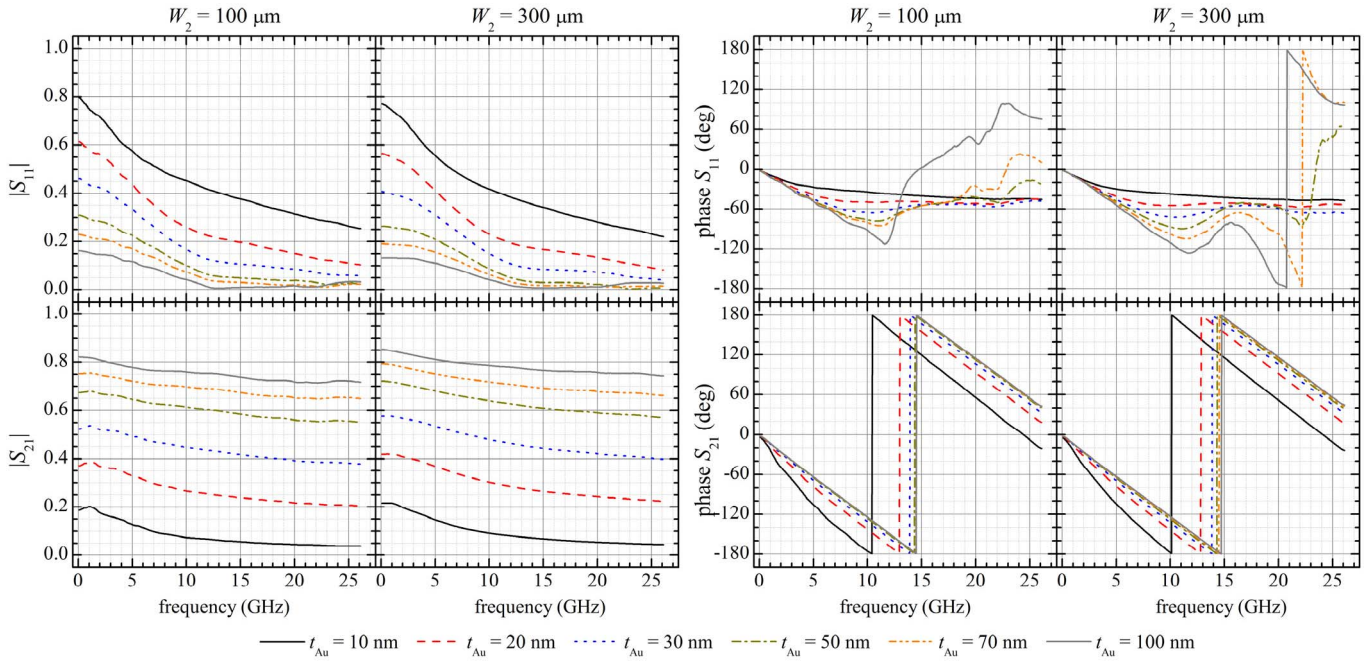

Fig. 4. Measured frequency characteristics (0.1–26 GHz) of the reflectance S_{11} and transmittance S_{21} of the 4-mm-long CPW segments with two values of finite-width ground planes W_2 for six gold metallization thicknesses t_{Au}.

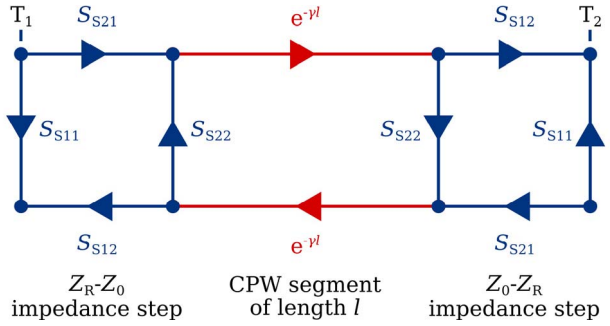

Fig. 5. Signal flow graph for a CPW segment placed between Ports 1 and 2 probes tips located at the reference planes T_1 and T_2, respectively.

their permittivity values. The metallization layout of these CPWs, particularly for $W_2 = 300$ μm, is similar to the metallization template of the line standards on the CRC-8. Based on these arguments, the contact-pad parasitic effects were neglected. Thus, an S-matrix measurement of single CPW segment enables the determination of this transmission line parameters. This method is the conventional one proposed in [34]. In this paper, the derivation of equations for the characteristic impedance and the propagation constant seems to be relatively cumbersome.

The signal flow graph presented in Fig. 5 is used to derive the equations necessary to find characteristic impedance Z_0 and propagation constant γ of the CPW. Based on the Mason rules [41] the signal flow graph can easily be reduced to show that the measured S-parameters at the planes T_1 and T_2 are as follows:

$$S_{11} = S_{S11}\frac{1-e^{-2\gamma l}}{1-S_{S11}^2 e^{-2\gamma l}} = S_{22} \tag{1}$$

$$S_{21} = S_{S21}^2\frac{e^{-\gamma l}}{1-S_{S11}^2 e^{-2\gamma l}} = S_{12} \tag{2}$$

where l is the length of the CPW segment, and the S-parameters of impedance step are given as follows:

$$S_{S11} = \frac{Z_0 - Z_R}{Z_0 + Z_R} = -S_{S22} \tag{3}$$

$$S_{S21} = \sqrt{1 - S_{S11}^2} = S_{S12} \tag{4}$$

where Z_R is the characteristic impedance of the probe.

Equation (1) can be solved for $\exp(-\gamma l)$ as follows:

$$e^{-\gamma l} = \sqrt{\frac{S_{S11} - S_{11}}{S_{S11}\cdot(1 - S_{S11}\cdot S_{11})}} \tag{5}$$

which is substituted into (2) to give a quadratic equation for the reflectance S_{S11}. Having S_{S11} and using (3), Z_0 is found in terms of the measured S-parameters as follows:

$$Z_0 = Z_R\sqrt{\frac{S_{21}^2 - (1+S_{11})^2}{S_{21}^2 - (1-S_{11})^2}}. \tag{6}$$

Finally, using (5), the propagation constant γ can be calculated, thus yielding both the attenuation constant α and the phase constant β as $\gamma = \alpha + j\beta$. Presentation of the determined propagation constant frequency characteristics is reasonable in terms of the attenuation constant and effective dielectric constant classically defined as $\varepsilon_{eff} = (\beta/\beta_{0P})^2$, where β_{0P} is the phase constant of the plane wave in the vacuum. The characteristic impedance, attenuation constant and effective dielectric constant characterizes the investigated transmission lines.

The parameters characterizing the measured CPWs: Z_0, α, and ε_{eff}, which were extracted in accordance with the above-described procedure from the S-parameters given in Fig. 4, are presented in Fig. 6. There is significant parameter variation both as a function of the metallization thickness and the

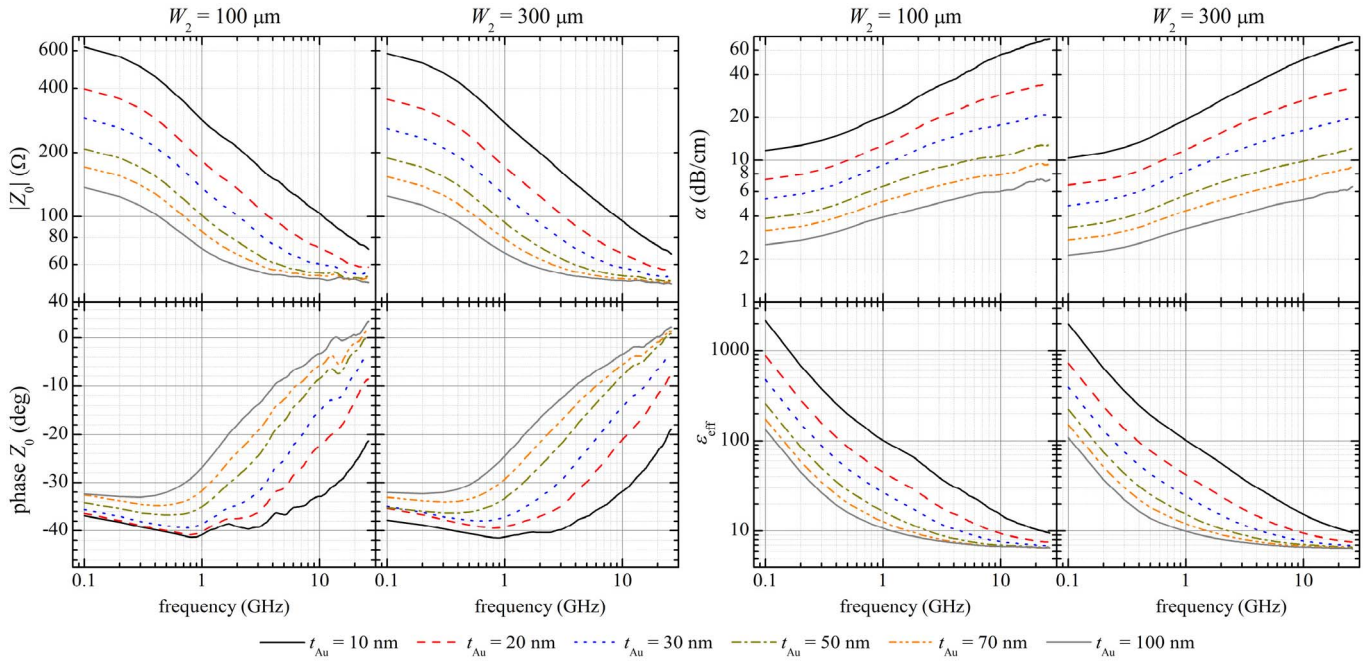

Fig. 6. Values of the module and phase of the characteristic impedance Z_0, values of the attenuation coefficient α and effective dielectric constant ε_{eff} of the CPWs for two values of width of outer metal strips (ground) in the 0.1–26-GHz frequency range as a function of thickness of the gold metallization t_{Au}.

frequency. Moreover, the parameter sensitivity on the metallization thickness changes monotonically with the frequency. For instance, the magnitude of the characteristic impedance decreases four times with increasing metallization thickness at 0.1 GHz but only 1.5 times at 26 GHz. The value of the effective dielectric constant decreases with increasing metallization thickness 16 times at 0.1 GHz and only 1.67 times at 26 GHz. The only parameter for which the sensitivity on the metallization thickness increases with the frequency is the attenuation constant, which changes 5 times at 0.1 GHz and 10 times at 26 GHz. The interpretation of the presented dependencies is difficult because, for frequencies up to 26 GHz, the measured CPWs with ultralow metallization thickness are in the intermediate range between dc and the skin-effect region. To model these lines, a complicated situation arises related to current distribution changes. Presenting elements of the distributed equivalent circuit model would exceed the limitations of this paper, but further information may be found [42].

Finally, the work by Haydl *et al.* [16] claims that when metal thickness t is less than 3 times the skin depth δ, the attenuation varies inversely with metal thickness t. This paper uses values that are obviously below δ; thus, we plot the attenuation ratio α for two frequencies $f = 1$ and 20 GHz as a function of layer thickness [Fig. 7(a)] and as a function of metallization sheet resistance $R_{\text{S,RF}}$ [Fig. 7(b)]. The following theoretical curve was fit to the experimental points as follows:

$$\alpha\,(f) = \frac{A}{t - t_0} \tag{7}$$

to achieve a good agreement. For $f = 20$ GHz, there is a direct inverse relationship between α and t ($t_0 = 0$), but for $f = 1$ GHz, a small correction to the thickness is required (t_0 of the order of a few nanometers). However, the presented results fully confirm the Haydl observations. Next, the frequency variation of the attenuation constant was examined to follow $\alpha\ (f) = \alpha_0 \bullet (f/1\ \text{GHz})^n$ dependence. The results are shown in Fig. 7(c) and (d), whereas the obtained parameters of the assumed model α_0 and exponent n are presented in Fig. 7(e) and (f), respectively. The theoretical curves closely follow the experimental data and intuitive decrease of the value of α_0 when the thickness increase is observed. The attenuation ratio $\alpha\ (f)$ and α_0 values are always lower for CPS with $W_2 = 300\ \mu$m than for $W_2 = 100\ \mu$m. This observation might be related to lower conductor losses for the wider ground strip. The exponent value n, expressing sensitivity of the attenuation constant on the frequency, decreases with increasing metallization thickness and is always smaller for $W_2 = 100\ \mu$m than for $W_2 = 300\ \mu$m. To check whether the data are similar to other literature reports, the data were extrapolated to $t = 250$ nm, and data from [17, Fig. 5] to $w/d = 0.5$ and $w = 100\ \mu$m (for the meaning of the symbols, please see the source paper). The results are presented in Table II. The results are just below the data from [17]. Further interpretation of the exponent n dependence on the gold metallization thickness will require detailed analysis of the RF current flow, which is beyond the scope of this paper.

TABLE II
EXPONENT n VALUES

#	exponent n	source
1	0.187	this work, $W_2 = 300$ μm, extrapolated to $t = 250$ nm
2	0.166	this work, $W_2 = 100$ μm, extrapolated to $t = 250$ nm
3	≈0.2	Ref [17], extrapolated to $w/d = 0.5$ and $w = 100$ μm

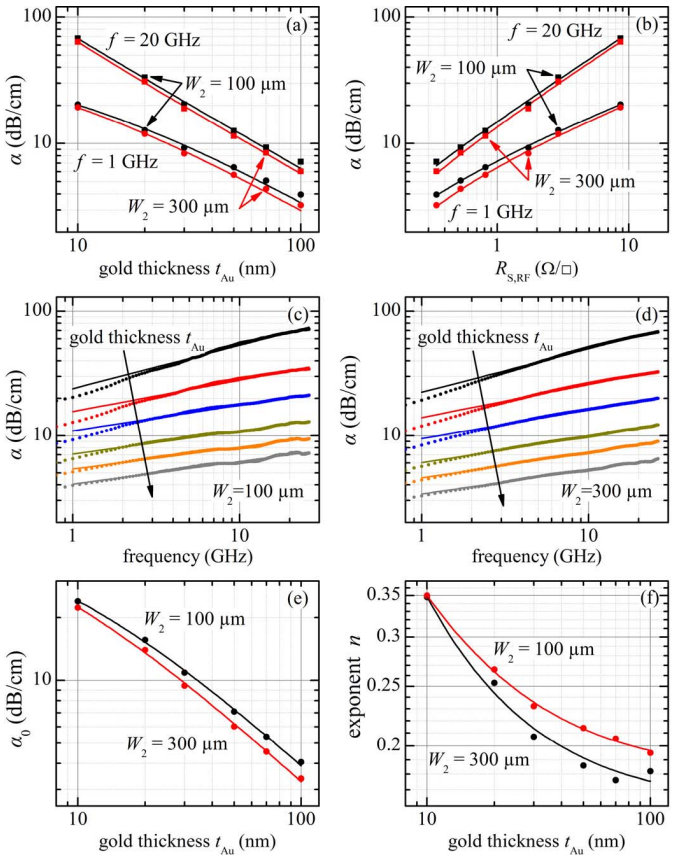

Fig. 7. Attenuation constant for two frequencies $f = 1$ and 20 GHz for $W_2 = 100$ μm and $W_2 = 300$ μm as a function of (a) gold metallization thickness t_{Au} and (b) metallization RF sheet resistance $R_{\mathrm{S,RF}}$. Theoretical dependence of attenuation constant $\alpha\ (f) = \alpha_0 \bullet (f/1\ \mathrm{GHz})^n$ fit for six gold metallization thickness values t_{Au} for (c) $W_2 = 100$ μm and (d) $W_2 = 300$ μm. Attenuation constants (dots) are the same as those shown in Fig. 6, whereas the parameters of the assumed model α_0 and exponent n are presented in (e) and (f), respectively. Solid lines in (b), (e), and (f) are guides for eye.

IV. Conclusion

We presented data that fully characterize the fabricated CPW with gold metallization thickness t_{Au} in the range of 10 to 100 nm in the frequency range from 0.1 to 26 GHz. We focused on the attenuation coefficient, which is directly and inversely dependent on the metallization thickness. We showed that the power dependence of the attenuation coefficient on the frequency adequately describes our data, and the value of the exponent n is in a good agreement with previously reported data.

References

[1] M. Tuo *et al.*, "Linear and nonlinear microwave characterization of CVD-grown graphene using CPW structure," in *Proc 9th EuCAP*, Apr. 2015, pp. 1–2.

[2] M. Tuo *et al.*, "Nonlinear microwave characterization of CVD grown graphene," *IEEE Antennas Wireless Propag. Lett.*, vol. 15, pp. 1557–1560, 2016.

[3] Z. R. Bu *et al.*, "Characteristics of trenched coplanar waveguide for SiMMIC applications," in *IEEE MTT-S Int. Microw. Symp. Dig.*, vol. 2. Jun. 1997, pp. 735–738.

[4] S. Yang *et al.*, "Characteristics of trenched coplanar waveguide for high-resistivity SI MMIC applications," *IEEE Trans. Microw. Theory Techn.*, vol. 46, no. 5, pp. 623–631, May 1998.

[5] W. Heinrich, J. Gerdes, F. J. Schmiickle, C. Rheinfelder, and K. Strohm, "Coplanar passive elements on Si substrate for frequencies up to 110 GHz," *IEEE Trans. Microw. Theory Techn.*, vol. 46, no. 5, pp. 709–712, May 1998.

[6] W. Durr, U. Erben, A. Schuppen, H. Dietrich, and H. Schumacher, "Investigation of microstrip and coplanar transmission lines on lossy silicon substrates without backside metallization," *IEEE Trans. Microw. Theory Techn.*, vol. 46, no. 5, pp. 712–715, May 1998.

[7] Y. Wu, S. Yang, H. S. Gamble, B. M. Armstrong, V. F. Fusco, and J. A. C. Stewart, "The effect of a SiO_2 interface layer on CPW lines and Schottky barrier diodes on HRS substrates," in *Topical Meeting Silicon Monolithic Integr. Circuits RF Syst. Dig.*, Sep. 1998, pp. 178–180.

[8] G. E. Ponchak, M. Matloubian, and L. P. B. Katehi, "A measurement-based design equation for the attenuation of MMIC-compatible coplanar waveguides," *IEEE Trans. Microw. Theory Techn.*, vol. 47, no. 2, pp. 241–243, Feb. 1999.

[9] Y. Wu, H. S. Gamble, B. M. Armstrong, V. F. Fusco, and J. A. C. Stewart, "SiO_2 interface layer effects on microwave loss of high-resistivity CPW line," *IEEE Microw. Guided Wave Lett.*, vol. 9, no. 1, pp. 10–12, Jan. 1999.

[10] H. S. Gamble, B. M. Armstrong, S. J. N. Mitchell, Y. Wu, V. F. Fusco, and J. A. C. Stewart, "Low-loss CPW lines on surface stabilized high-resistivity silicon," *IEEE Microw. Guided Wave Lett.*, vol. 9, no. 10, pp. 395–397, Oct. 1999.

[11] D. Lederer and J. P. Raskin, "Substrate loss mechanisms for microstrip and CPW transmission lines on lossy silicon wafers," in *IEEE MTT-S Int. Microw. Symp. Dig.*, vol. 2. Jun. 2002, pp. 685–688.

[12] E. Duraz *et al.*, "CPW on silicon substrates: Propagation constant modeling and substrate free carriers contribution," in *Proc. 35th Eur. Microw. Conf.*, vol. 2. Oct. 2005, pp. 885–888.

[13] T. Makita, I. Tamai, and S. Seki, "Coplanar waveguides on high-resistivity silicon substrates with attenuation constant lower than 1 dB/mm for microwave and millimeter-wave bands," *IEEE Trans. Electron Devices*, vol. 58, no. 3, pp. 709–715, Mar. 2011.

[14] R. L. Wang, Y. K. Su, and C. J. Chen, "Transmission performances of CPW lines on a laser-crystallization polysilicon passivated high-resistivity silicon substrate," *IEEE Trans. Compon., Packag., Manuf. Technol.*, vol. 2, no. 5, pp. 847–851, May 2012.

[15] W. H. Haydl, T. Kitazawa, J. Braunstein, R. Bosch, and M. Schlechtweg, "Millimeter-wave coplanar transmission lines on gallium arsenide indium phosphide and quartz with finite metallization thickness," in *IEEE MTT-S Int. Microw. Symp. Dig.*, vol. 2. Jul. 1991, pp. 691–694.

[16] W. H. Haydl, J. Braunstein, T. Kitazawa, M. Schlechtweg, P. Tasker, and L. F. Eastman, "Attenuation of millimeterwave coplanar lines on gallium arsenide and indium phosphide," in *IEEE MTT-S Int. Microw. Symp. Dig.*, vol. 1. Jun. 1992, pp. 349–352.

[17] W. H. Haydl, "Experimentally observed frequency variation of the attenuation of millimeter-wave coplanar transmission lines with thin metallization," *IEEE Microw. Guided Wave Lett.*, vol. 2, no. 8, pp. 322–324, Aug. 1992.

[18] G. E. Ponchak, E. M. Tentzeris, and L. P. B. Katehi, "Characterization of finite ground coplanar waveguide with narrow ground planes," *Int. J. Microcircuits Electron. Packag.*, vol. 20, no. 2, pp. 167–173, 1997.

[19] M. Ramazani, H. Miladi, M. Shahabadi, and S. Mohajerzadeh, "Loss measurement of aluminum thin-film coplanar waveguide (CPW) lines at microwave frequencies," *IEEE Trans. Electron Devices*, vol. 57, no. 8, pp. 2037–2040, Aug. 2010.

[20] A. C. Reyes, S. M. El-Ghazaly, S. Dorn, M. Dydyk, and D. K. Schroder, "Silicon as a microwave substrate," in *IEEE MTT-S Int. Microw. Symp. Dig.*, vol. 3. May 1994, pp. 1759–1762.

[21] A. C. Reyes, S. M. El-Ghazaly, S. J. Dorn, M. Dydyk, D. K. Schroder, and H. Patterson, "Coplanar waveguides and microwave inductors on silicon substrates," *IEEE Trans. Microw. Theory Techn.*, vol. 43, no. 9, pp. 2016–2022, Sep. 1995.

[22] A. C. Reyes, S. M. El-Ghazaly, S. Dorn, M. Dydyk, D. K. Schroder, and H. Patterson, "High resistivity SI as a microwave substrate," in *Proc. 46th Electron. Compon. Technol. Conf.*, May 1996, pp. 382–391.

[23] C. Warns, W. Menzel, and H. Schumacher, "Transmission lines and passive elements for multilayer coplanar circuits on silicon," *IEEE Trans. Microw. Theory Techn.*, vol. 46, no. 5, pp. 616–622, May 1998.

[24] S. Tan *et al.*, "CPW transmission lines on silicon supporting 10 G/40 G InP EAM chip on carrier applications," in *Proc. 53rd Electron. Compon. Technol. Conf.*, May 2003, pp. 308–311.

[25] B. Rong, J. N. Burghartz, L. K. Nanver, B. Rejaei, and M. van der Zwan, "Surface-passivated high-resistivity silicon substrates for RFICs," *IEEE Electron Device Lett.*, vol. 25, no. 4, pp. 176–178, Apr. 2004.

[26] J. Krupka, W. Karcz, P. Kamiński, and L. Jensen, "Electrical properties of as-grown and proton-irradiated high purity silicon," *Nucl. Instrum. Methods Phys. Res. B, Beam Interact. Mater. At.*, vol. 380, pp. 76–83, Aug. 2016.
[27] J. Krupka, "Contactless methods of conductivity and sheet resistance measurement for semiconductors, conductors and superconductors," *Meas. Sci. Technol.*, vol. 24, no. 6, pp. 1–13, 2013.
[28] E. V. Barnat, D. Nagakura, P.-I. Wang, and T.-M. Lu, "Real time resistivity measurements during sputter deposition of ultrathin copper films," *J. Appl. Phys.*, vol. 91, no. 3, p. 1667, 2002.
[29] M. C. Salvadori, L. L. Melo, A. R. Vaz, R. S. Wiederkehr, F. S. Teixeira, and M. Cattani, "Platinum and gold thin films deposited by filtered vacuum arc: Morphological and crystallographic grain sizes," *Surf. Coat. Technol.*, vol. 200, no. 9, p. 2965, 2006.
[30] *WinCal XE Version 4.5*, Cascade Microtech, Beaverton, OR, USA, 2011.
[31] L. Hayden, "An enhanced line-reflect-reflect-match calibration," in *67th ARFTG Conf. Dig.*, Jun. 2006, pp. 143–149.
[32] "Calibration tools: Achieving consistent parameter extraction for advanced RF devices," Cascade Microtech, Beaverton, OR, USA, Appl. Note CALTOOL-AN-0612, 2012. [Online]. Available: https://www.cascademicrotech.com/files/CalParaExtraction_AN.pdf
[33] (2009). "PNA-X network analyzer N5242A data sheet and technical specifications," Agilent Technol., Santa Clara, CA, USA, Tech. Rep. N5242-90007. [Online]. Available: http://cp.literature.agilent.com/litweb/pdf/N5242-90007.pdf
[34] W. R. Eisenstadt and Y. Eo, "S-parameter-based IC interconnect transmission line characterization," *IEEE Trans. Compon., Hybrids, Manuf. Technol.*, vol. 15, no. 4, pp. 483–490, Aug. 1992.
[35] R. B. Marks and D. F. Willians, "Interconnection transmission line parameter characterization," in *40th ARFTG Conf. Dig.*, Dec. 1992, pp. 88–95.
[36] D. F. Williams and R. B. Marks, "Accurate transmission line characterization," *IEEE Microw. Guided Wave Lett.*, vol. 3, no. 8, pp. 247–249, Aug. 1993.
[37] D. C. DeGroot, D. K. Walker, and R. B. Marks, "Impedance mismatch effects on propagation constant measurements," in *IEEE 5th Topical Meeting, Elect. Perform. Electron. Packag. Dig.*, Dec. 1996, pp. 141–143.
[38] Y. C. Shih and K. S. Kong, "Accurate broadband characterization of transmission lines," in *IEEE MTT-S Int. Microw. Symp. Dig.*, vol. 2. Jun. 1998, pp. 933–936.
[39] G. Carchon and B. Nauwelaers, "Accurate transmission line characterisation on high and low-resistivity substrates," *IEE Proc. Microw. Antennas Propag.*, vol. 148, no. 5, pp. 285–290, Oct. 2001.
[40] J. Balachandran, S. Brebels, G. Carchon, W. De Raedt, B. Nauwelaers, and E. Beyne, "Accurate broadband parameter extraction methodology for S-parameter measurements," in *Proc. 9th IEEE Workshop Signal Propag. Interconnects*, May 2005, pp. 57–60.
[41] S. J. Mason and H. J. Zimmermann, *Electronic Circuits, Signals and Systems*. New York, NY, USA: Wiley, 1960, ch. 4.
[42] W. Heinrich, "Quasi-TEM description of MMIC coplanar lines including conductor-loss effects," *IEEE Trans. Microw. Theory Techn.*, vol. 41, no. 1, pp. 45–52, Jan. 1993.

Jarosław Judek, photograph and biography not available at the time of publication.

Arkadiusz P. Gertych, photograph and biography not available at the time of publication.

Michał Świniarski, photograph and biography not available at the time of publication.

Mariusz Zdrojek, photograph and biography not available at the time of publication.

Jerzy Krupka, photograph and biography not available at the time of publication.

Jerzy K. Piotrowski, photograph and biography not available at the time of publication.